NANO LETTERS

Letter

pubs.acs.org/NanoLett

Carbon Nanotube Active-Matrix Backplanes for Mechanically Flexible Visible Light and X-ray Imagers

Toshitake Takahashi,[†,‡,§,■] Zhibin Yu,[†,‡,§,■] Kevin Chen,[†,‡,§] Daisuke Kiriya,[†,‡,§] Chuan Wang,[†,‡,§,⊥] Kuniharu Takei,[†,‡,§,¶] Hiroshi Shiraki,[†,‡,§] Teresa Chen, Biwu Ma,[§,∥,□] and Ali Javey[†,‡,§,#,*]

[†]Electrical Engineering and Computer Sciences and [‡]Berkeley Sensor and Actuator Center, University of California, Berkeley, California 94702, United States

[§]Materials Sciences Division and [∥]The Molecular Foundry, Lawrence Berkeley National Laboratory, Berkeley, California 94720, United States

[#]Department of Chemistry, Faculty of Science, King Abudulaziz University, Jeddah 21589, Saudi Arabia

Supporting Information

ABSTRACT: We report visible light and X-ray imagers on lightweight and mechanically flexible plastic substrates. The process involves solution processing of organic photodetectors on top of an active-matrix backplane consisting of carbon nanotube thin-film transistors. The system takes advantage of the high mobility of nanotube transistors for low operating voltages and efficient light absorption of organic bulk-heterojunctions for high imaging sensitivity. With this highly scalable process scheme, 18 × 18 pixel-array flexible imagers (physical size of 2 cm × 1.5 cm) with high performance are successfully demonstrated. In addition, as the absorption peak of the adopted organic photodiodes covers the green band of the light spectrum, X-ray imaging is readily demonstrated by placing a scintillator film on top of the flexible imagers.

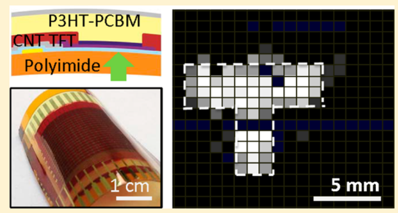

KEYWORDS: *Thin film transistors, single-walled carbon nanotubes, organic photodiodes, electronic skin, bendable, imaging*

Recent advancements in the processing of electronically monodisperse carbon nanotubes have enabled the exploration of a wide range of functional devices based on random networks of nanotubes.[1,2] In particular, thin film transistors (TFTs) using solution-processed semiconductor-enriched nanotubes have been demonstrated to exhibit excellent electrical properties with high uniformity on both rigid and flexible substrates.[3−7] High hole mobilites of up to 50 $cm^2/(V\ s)$ with high I_{on}/I_{off} of up to 10^6 have been reported for nanotube TFTs.[4] These reported performances clearly present an advantage over a-Si and organic semiconductor-based devices that often exhibit mobilities that are lower by over 2 orders of magnitude as compared to those of nanotube networks. In addition, large-area processing of nanotube TFTs using inkjet and roll-to-plate processing have already been demonstrated.[8−10] Thereby, nanotube TFTs are particularly promising for low-power active matrix backplanes on a wide range of substrates, including mechanically flexible plastics. In this regard, nanotube active matrix backplanes have recently been successfully integrated with pressure sensors for the fabrication of electronic skins[3,11] and organic light-emitting diodes for flexible displays.[11] The high hole mobility of nanotube TFTs enables low voltage operation of the backplanes,[3,4] which is important for enabling system-level, practical applications.

Here, we extend the use of nanotube backplanes for another major application domain involving large-area flexible imagers.[12,13] We monolithically integrate organic photodetectors (OPDs) made of regioregular poly(3-hexylthiophene) (P3HT) and [6,6]-phenyl C61-butyric acid methyl ester (PCBM) on top of a nanotube backplane consisting of an 18 × 18 pixel array (physical size of 2 cm × 1.5 cm). The absorption spectrum of P3HT/PCBM bulk-heterojunction photodetectors is optimal for visible light imaging applications.[14] Furthermore, by integrating a Gd_2O_2S/Tb (GOS) scintillator film[15] on top of the imager, a mechanically flexible X-ray detector[16] is demonstrated. In this system, the scintillator film converts incident X-rays into visible photons with an energy of ∼2.27 eV matching the peak absorption wavelength of the OPDs. The enabled devices exhibit high performance in terms of imaging sensitivity, response time, and uniformity. This work presents a practical platform for a new form of flexible sensor networks for large-area imaging applications.

Fabrication procedure for our imagers is briefly described in Figure 1a. First, polyimide (PI; thickness of ∼24 μm) is spin-coated on a Si supporting wafer, followed by curing on a hot plate at 300 °C for 1h.[3] Ni gate (G) electrodes are then fabricated using photolithography, evaporation, and lift-off. Atomic layer deposition of Al_2O_3 (∼70 nm) sandwiched between evaporated SiO_x (∼ 10 nm) layers is performed to serve as the gate dielectric layer. Next, 99% semiconductor-enriched single-walled carbon nanotube (SWNT) solution

Received: August 10, 2013
Revised: October 7, 2013
Published: October 21, 2013

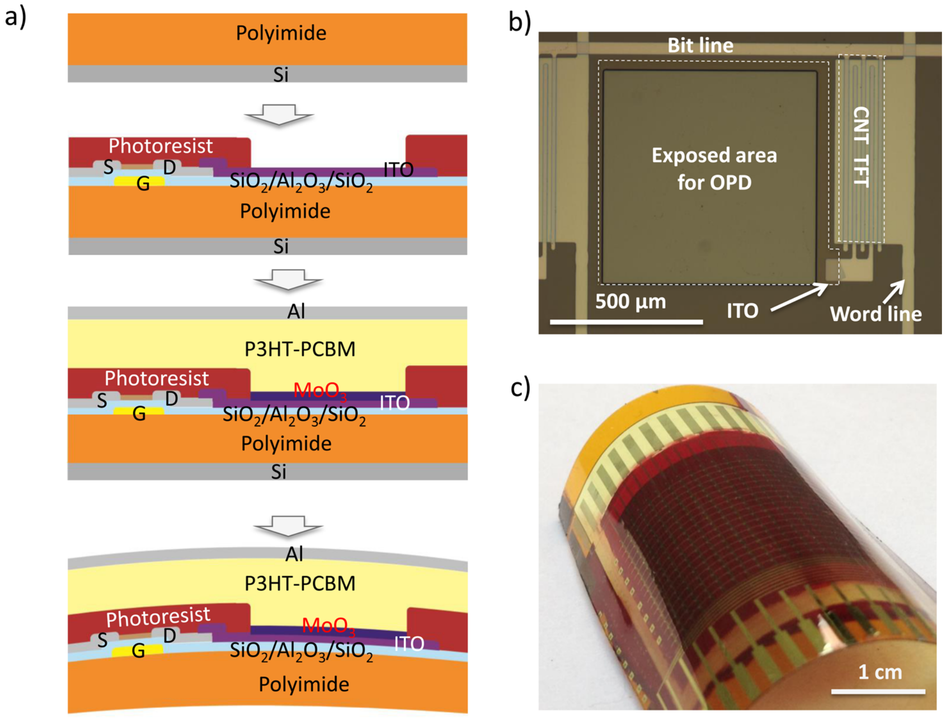

Figure 1. Fabrication of mechanically flexible imagers. (a) Step-by-step fabrication process flow. (b) Optical image of a single pixel after the completion of the nanotube TFT process. (c) Optical image of a fully fabricated imager.

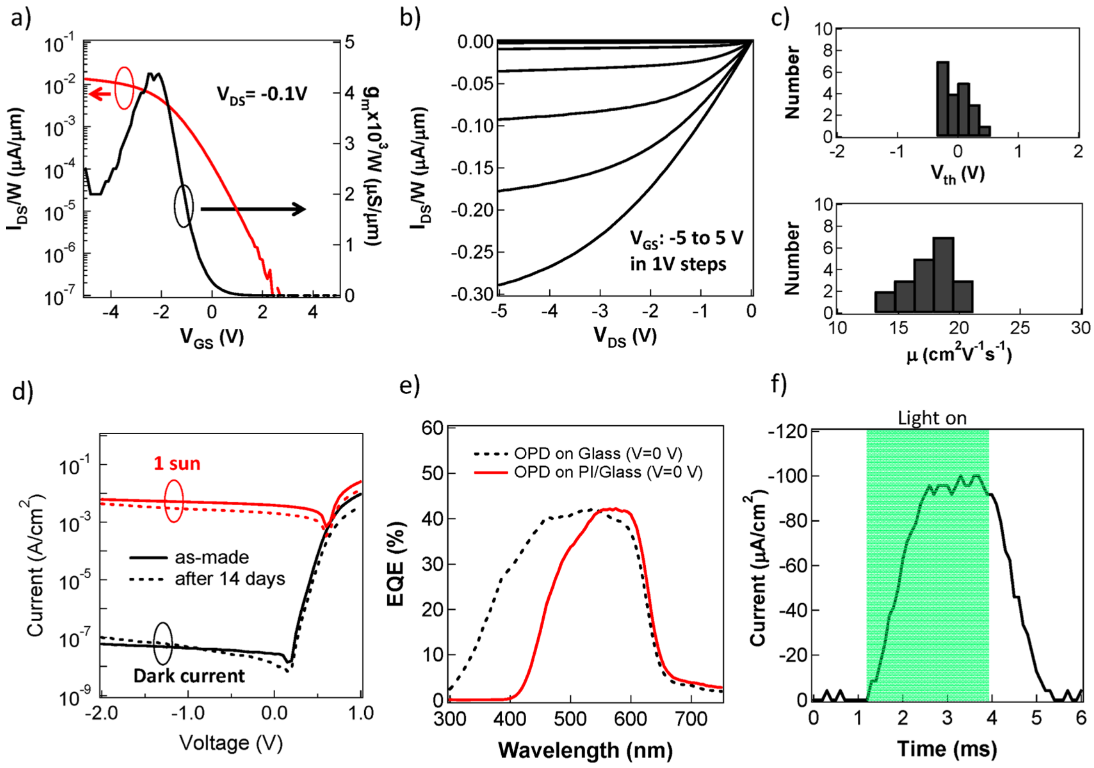

Figure 2. Electrical and optical characteristics of stand-alone TFTs and OPDs. (a) Channel width normalized drain current versus gate voltage characteristic at a drain voltage of −0.1 V. The corresponding transconductance as a function of gate voltage is also shown. Channel length and width are 30 and 2000 μm, respectively. (b) Channel-width normalized $I_{DS}-V_{DS}$ characteristics measured for applied gate voltages of −5 to 5 V in 1 V steps. (c) Histograms of mobility and threshold voltage for 20 randomly chosen TFTs across the substrate. (d) Current−voltage characteristics of an organic photodiode measured under AM1.5 1-sun and dark condition (solid lines). Same device is measured again after exposure to ambient atmosphere for 14 days (dashed lines). (e) External quantum efficiency between 300 and 750 nm for an organic photodiode on PI (red line) and glass (black dashed line) substrates. (f) Time response of the photocurrent at a reverse bias of 2 V for an incident light with λ = 535 nm and intensity of 1000 μW/cm^2.

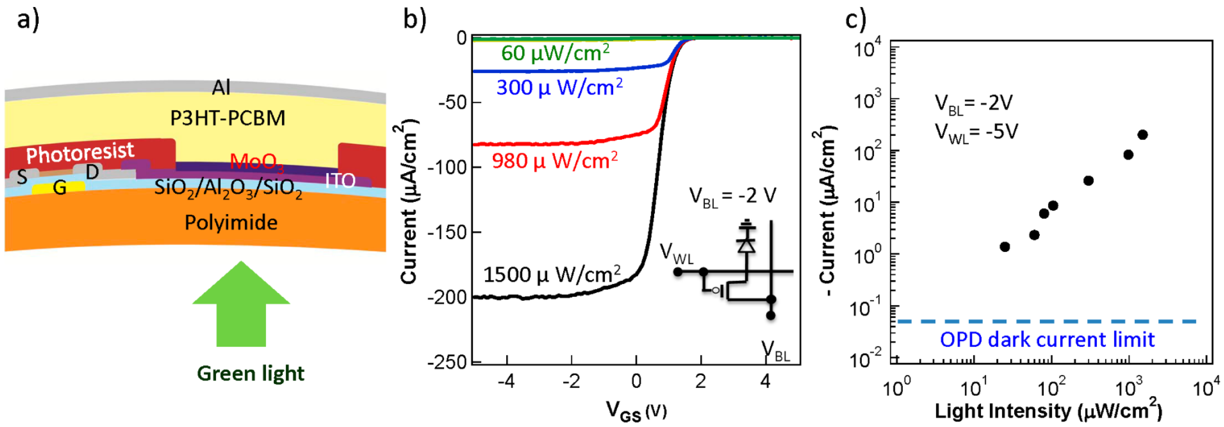

Figure 3. Characterization of individual pixels. (a) Cross-sectional schematic of a single pixel. Light is exposed from the PI side. (b) Transfer characteristics of one pixel under various light intensities (λ = 535 nm). The inset shows the circuit schematic of a pixel. (c) Photocurrent response of a pixel at V_{GS} = −5 V and V_{BL} = −2 V as a function of incident light intensity.

(NanoIntegris, Inc.) is drop-casted on a poly-L-lysine functionalized surface,[3] followed by Ti (0.5 nm)/Pd (40 nm) source/drain (S/D) electrode formation by photolithography, metallization, and lift-off. Subsequently, O_2 plasma (60 W, 2 min) treatment is performed to burn out nanotube films outside the active regions. Next, indium tin oxide (ITO) pads (thickness of ~80 nm) are deposited using sputtering to serve as the anode of the subsequently fabricated photodiodes. Each ITO pad is in electrical contact with the drain electrode of the corresponding TFTs. A photoresist (S1818, ~2 μm) layer is then spin-coated to encapsulate SWNT TFTs with only the ITO regions exposed (Figure 1b). The sample is baked on a hot plate at 200 °C for 30 min to enhance ITO performance as well as hardening the photoresist in order to not be dissolved in organic solvents in the subsequent process steps. Next, a ~9 nm thick MoO_3 hole transportation layer[17,18] is thermally evaporated after cleaning the ITO surface with ozone treatment. The organic semiconductor film (80 mg/mL mixture of P3HT and PCBM with the weight ratio of 1:1 in chlorobenzene[19]) is spin-coated at 1000 rpm for 30 s. The film thickness is ~500 nm. Finally, Al is evaporated through a shadow mask to form the cathode electrode, followed by a thermal anneal at 150 °C for 10 min in order to form a bicontinuous heterojunction network in the organic semiconductor film.[20] The PI substrate with the TFTs and photodiodes on top is then mechanically peeled off from the supporting Si substrate to form mechanically flexible imagers. The optical image of the fully fabricated device bent to a curvature radius of ~1 cm is shown in Figure 1c.

We first studied the electrical characteristics of individual nanotube TFTs (L ~ 30 μm, W ~ 2000 μm) and organic photodiodes on a flexible PI substrate. The channel width normalized transfer ($I_{DS}/W-V_{GS}$) and transconductance ($g_m/W-V_{GS}$) characteristics from a representative TFT measured at V_{DS} = 0.1 V are shown in Figure 2a. As previously reported,[3−5,7] solution-based nanotube processing produces uniform device characteristics in terms of on-current (I_{ON}), transconductane (g_m), on/off ratio (I_{ON}/I_{OFF}), threshold voltage (V_{th}), and mobility (μ). Using extracted peak transconductance, the field effect mobility is calculated as $\mu = (L/V_{DS}C_{ox})(g_m/W)$, where the parallel plate model is used to calculate the gate oxide capacitance, C_{ox} = 6.43 × 10^{-8} [F/cm²]. The calculated mobility is ~20 cm²/(V s), which is comparable to previously reported values, although this value is underestimated by ~2× due to the overestimation of the gate capacitance since the entire surface is not covered by SWNTs.[4] More rigorous $C-V$ analysis is required to extract actual value as performed in our previous study.[4] The output characteristics measured at V_{GS} = −5 to 5 V in 1 V steps of a representative TFT is shown in Figure 2b, exhibiting clear metal-oxide-semiconductor field-effect transistor (MOSFET)-like behavior. In this work, we are interested in developing large-area sensor networks with the size of the system being on the cm scale. In this regard, device performance uniformity is essential. To examine the uniformity, 20 TFTs are randomly chosen across the substrate, and the histogram of calculated mobility and threshold voltage measured at V_{DS} = 0.1 V are shown in Figure 2c. The average mobility and threshold voltage is 17.4 ± 2.2 cm²/(V s) and −0.03 ± 0.22 V, respectively. This uniformity is sufficient for the fabrication of an imager which is discussed later in this manuscript.

Optical characteristics of standalone organic photodiodes on flexible substrates are also characterized. Here, the light is illuminated from the back-side; through the PI substrate. Figure 2d shows $I-V$ characteristics measured under dark and AM1.5 1-sun illumination conditions. The photocurrent at a reverse bias voltage of 1 V is ~5 mA/cm². The dark current for the same reverse bias voltage is ~42 nA/cm², which is close to the state-of-the-art OPDs reported in literature (~10 nA/cm²).[21] To further lower the dark current, thickness engineering and device structure optimization, such as adding an electron transport layer on the cathode side, are needed.[22] Nevertheless, the reverse bias current is low with light (1-sun) to dark current ratio of ~10^5 at −1 V (Figure 2d). Furthermore, high device stability to ambient air up to 14 days is observed even without any encapsulation layer (Figure 2d).[23] Notably, the devices exhibit excellent mechanical flexibility with minimal change in the $I-V$ characteristics as a function of bending (Supporting Information, Figure S1).

External quantum efficiency (EQE) was measured for the generated photocurrent in the wavelength range of 300 − 750 nm as shown in Figure 2e. A photodiode fabricated using the same process but on a glass substrate (instead of PI) is also added as a reference. The light absorption by the PI film occurs at wavelengths of <400 nm, which does not significantly affect visible light photoresponse of the diodes. The peak EQE is observed at ~580 nm, which matches well with the emission spectrum of the GOS for eventual X-ray imaging applications as

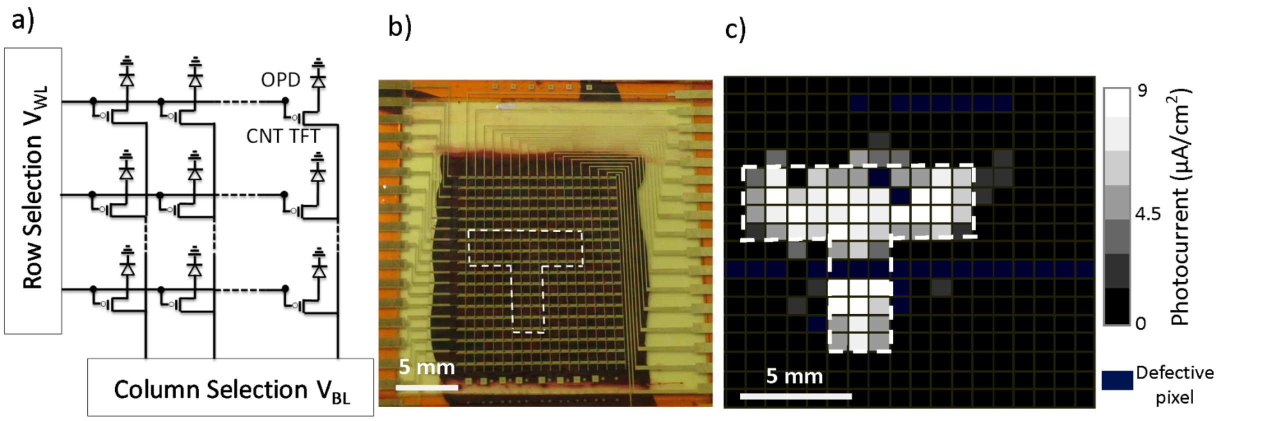

Figure 4. Flexible visible light imagers. (a) Circuit schematic of the imager. (b) Optical photograph of a fully fabricated imager (18 × 18 pixels). The imager is exposed to light with an intensity of 100 μW/cm^2 and λ = 535 nm through a "T"-shaped shadow mask (the mask is not shown). (c) The corresponding two-dimensional intensity profile obtained by measuring the photocurrent of the pixels. The character "T" is readily imaged by the device.

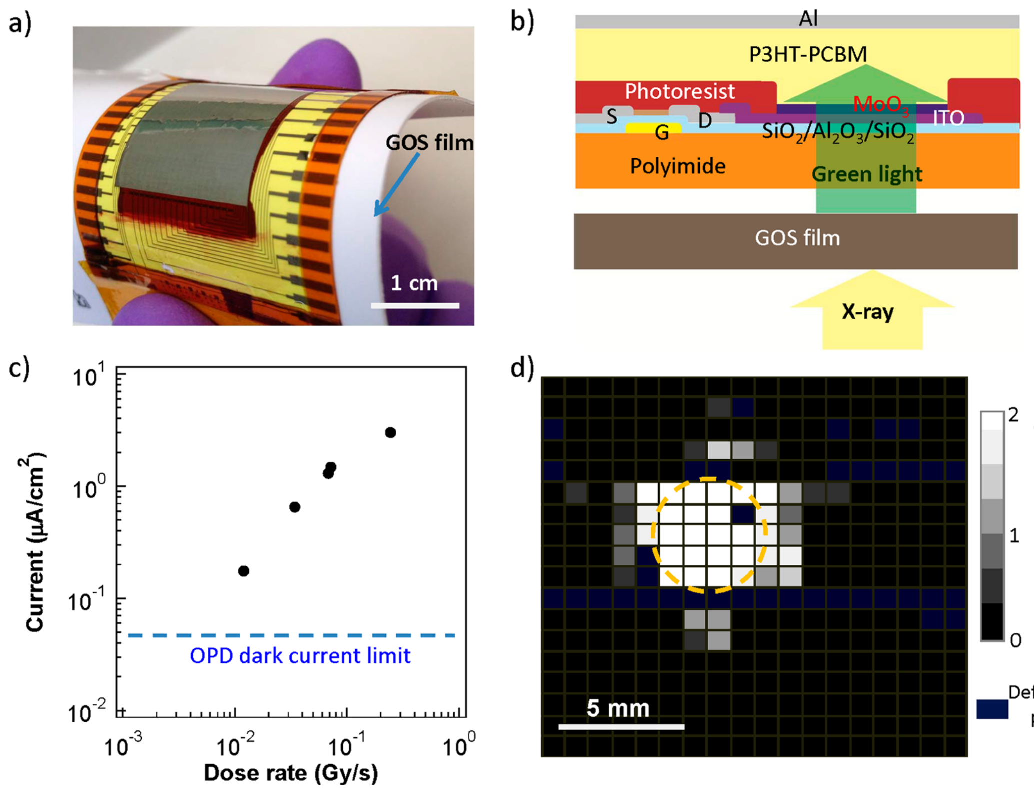

Figure 5. Flexible X-ray imagers. (a) Optical photograph of an imager placed on top of a GOS film used for X-ray detection. (b) Cross-sectional schematic of one pixel. X-rays are irradiated onto the GOS film, and emitted green light is detected by the OPDs of each pixel. (c) Measured current from one pixel at a reverse bias of 2 V as a function of X-ray dose rate. (d) Spatial mapping when a circle-shaped (diameter of 4 mm) X-ray source is projected with a dose rate of 100 mGy/s.

discussed later in this paper. Figure 2f shows the transient photocurrent response at a reverse bias of 2 V to an incident light (λ = 535 nm, 1000 μW/cm^2) chopped at 42 Hz. The response is characterized by a rise time, $\tau_r \sim 1$ ms and a decay time, $\tau_d \sim 1$ ms, which are compatible to other reported organic photodiodes on flexible substrates.[21]

Next, organic photodiodes are integrated with SWNT TFTs backplane to form 18 × 18 pixel arrays (physical size is 2 cm × 1.5 cm). Each pixel is composed of one organic photodiode in series with a nanotube TFT, and the word line (V_{WL}) and bit line (V_{BL}) voltages are applied to address each pixel. The cross sectional schematic of one pixel is shown in Figure 3a with the corresponding circuit diagram shown in the inset of Figure 3b. The integrated pixel response is characterized by measuring the current between the cathode of the photodiode and the source of the SWNT TFT at $V_{BL} = -2$ V as a function of V_{WL} (i.e., gate voltage of the TFT). Here, the wavelength of the incident light is λ = 535 nm and the intensity is varied from 0 to 1500 μW/cm^2 (Figure 3b). Strong photoresponse is clearly observed for $V_{GS} < 0$ V, corresponding to the ON-state of the TFTs. The dark current of photodiode limits the overall current flow of the pixel, which is needed for proper operation. The log−log plot of current at $V_{BL}= -2$ V and $V_{WL} = -5$ V as a function of incident light intensity is plotted in Figure 3c. Clearly, a linear-response is observed with a slope of ~0.15 μA/μW, corresponding to the sensitivity of the sensor. This linear response is highly desirable for the practical use of the sensors. The sensitivity value of our devices is within ~2× of the best value reported in the literature for OPDs.[24] The lowest detectable light intensity is ~10 μW/cm^2, corresponding to ~100 nA/cm^2 which is limited by the OPD dark current.

To demonstrate the imaging functionality of the pixel array (Figure 4a), the device is exposed to an incident light with λ = 535 nm and intensity of ~100 μW/cm^2 through a "T"-shaped shadow mask (Figure 4b). The current of each pixel is measured by applying $V_{BL} = -2$ V and $V_{WL} = -5$ V, while the rest of pixels are turned off by applying $V_{WL} = 5$ V. As depicted in Figure 4c, the irradiated light profile is successfully obtained by electronic readout. The yield of functional pixels is ~90% with the defective pixels mainly caused by fabrication failure such as poor lift-off of S/D or G electrodes. This high yield indicates that the lab-scale process scheme used here for both nanotube TFTs and organic photodiodes is not only scalable but also reliable. The pixel size used in this work is set to ~1 mm^2. This reduces the total number of pixels, thereby, simplifying the measurement. In the future, higher resolution is easily attainable by reducing the pixel dimensions down to the photolithography limit (i.e., micrometers scale).

The fabricated imager can also be readily used for X-ray imaging by laminating a scintillator film on the substrate (facing the incident X-ray) as shown in Figure 5a. In this indirect X-ray detection approach, a GOS scintillator film is used to convert X-ray photons into green light with an emission peak of ~545 nm,[15] which is then detected by the photodiodes in the imager. The cross sectional schematic of a single pixel is shown in Figure 5b. As discussed in Figure 2e, the peak EQE of P3HT/PCBM photodiodes perfectly matches the green fluorescence emission at 545 nm of the GOS film. Figure 5c is a log−log plot of measured current of a single pixel as a function of incident X-ray dose rate, showing a linear correlation down to ~10 mGys^{-1} (corresponding to a photocurrent of ~200 nA/cm^2). This is close to the resolution limit set by the dark current of our photodiodes. Further improvement in photodiode quality as mentioned above would make the pixel response to lower dose rates feasible. With the protection of the GOS film, the pixels remain stable after exposure to X-ray source. Experimentally, we observed both dark and photo currents are nearly unchanged after exposure to ~300 Gy, which was the maximum total dose tested in the measurements. Finally, spatial mapping is performed by using a dose rate of ~100 mGys^{-1} generated by a circle-shaped (~4 mm in diameter) X-ray source (General Electric, model XRD4 operated at 20 kV and 25 mA). The spatial profiling of the incident X-ray is electrically resolved using the fabricated imager (Figure 5d). The results demonstrate the utility of this flexible system as a lightweight and portable X-ray imager that can readily be wrapped around body parts for future medical imaging applications.

In summary, we have successfully demonstrated the use of solution-processed nanotube TFTs as the active-matrix backplane for mechanically flexible imagers with high performance. Both visible light and X-ray detections are demonstrated. Moving forward, the large-area visible light imagers may provide a new platform for the development of interactive surfaces and displays[3,25−28] that can be laminated on different objects and spatially map hand and body movement as a user-interface. In the future, integration of microlens on each pixel needs to be explored for tuning the depth-of-focus and resolution. Imaging resolution was not emphasized in this work in order to minimize the total number of pixels for ease of electronic readout of the backplane. In the future, the pixel resolution can be readily scaled down to micrometer-scale if photolithography based processing is used. Finally, the scalability of the system can be further enhanced by exploring printing based fabrication technologies, especially given the recent advancements[8−10] in fully printed nanotube TFTs on plastics with excellent performance.

■ ASSOCIATED CONTENT

Ⓢ Supporting Information

Mechanical flexibility of organic photodiodes. This material is available free of charge via the Internet at http://pubs.acs.org.

■ AUTHOR INFORMATION

Corresponding Author

*E-mail: ajavey@eecs.berkeley.edu.

Present Addresses

⊥Electrical and Computer Engineering, Michigan State University, East Lansing, Michigan 48824.

¶Physics and Electronics, Osaka Prefecture University, Osaka 588−8531, Japan.

□Chemical and Biomedical Engineering, Florida State University, Tallahassee, Florida 32310.

Author Contributions

■T.T. and Z.Y. contributed equally.

Notes

The authors declare no competing financial interest.

■ ACKNOWLEDGMENTS

We thank Dr. R. Gupta of Harvard University for valuable discussions and providing the GOS films. This work was supported by NSF NASCENT Center. Work at the Molecular Foundry (photodiode fabrication) was supported by the Office of Science, Office of Basic Energy Sciences, of the U.S. Department of Energy under Contract No. DE-AC02-05CH11231. Measurements of the photodiodes were performed in the Electronic Materials laboratory, LBNL, which is supported by the Director, Office of Science, Office Basic Energy Sciences, Division of Materials Sciences and Engineering, of the U.S. Department of Energy.

■ REFERENCES

(1) Ghosh, S.; Bachilo, S. M.; Weisman, R. B. *Nat. Nanotechnol.* **2010**, *5*, 443−450.

(2) Green, A. A.; Hersam, M. C. *Adv. Mater.* **2011**, *23*, 2185−2190.

(3) Takahashi, T.; Takei, K.; Gillies, A. G.; Fearing, R. S.; Javey, A. *Nano Lett.* **2011**, *11*, 5408−5413.

(4) Wang, C.; Chien, J. C.; Takei, K.; Takahashi, T.; Nah, J.; Niknejad, A. M.; Javey, A. *Nano Lett.* **2012**, *12*, 1527−1533.

(5) Wang, C.; Zhang, J. L.; Ryu, K. M.; Badmaev, A.; De Arco, L. G.; Zhou, C. W. *Nano Lett.* **2009**, *9*, 4285−4291.

(6) Wang, C.; Takei, K.; Takahashi, T.; Javey, A. *Chem. Soc. Rev.* **2013**, *42*, 2592−2609.

(7) Wang, C. A.; Zhang, J. L.; Zhou, C. W. *ACS Nano* **2010**, *4*, 7123−7132.

(8) Chen, P. C.; Fu, Y.; Aminirad, R.; Wang, C.; Zhang, J. L.; Wang, K.; Galatsis, K.; Zhou, C. W. *Nano Lett.* **2011**, *11*, 5301−5308.

(9) Lau, P. H.; Takei, K.; Wang, C.; Ju, Y.; J., K.; Yu, Z.; Takahashi, T.; Cho, G.; Javey, A. *Nano Lett.* **2013**, *13* (8), 3864−3869.

(10) Ha, M. J.; Xia, Y.; Green, A. A.; Zhang, W.; Renn, M. J.; Kim, C. H.; Hersam, M. C.; Frisbie, C. D. *ACS Nano* **2010**, *4*, 4388−4395.
(11) Wang, C.; Hwang, D.; Yu, Z.; Takei, K.; Park, J.; Chen, T.; Ma, B.; Javey, A. *Nat. Mater.* **2013**, *12*, 899−904.
(12) Someya, T.; Kato, Y.; Iba, S.; Noguchi, Y.; Sekitani, T.; Kawaguchi, H.; Sakurai, T. *IEEE Trans. Electron Devices* **2005**, *52*, 2502−2511.
(13) Tong, X. R.; Forrest, S. R. *Org. Electron.* **2011**, *12*, 1822−1825.
(14) Mihailetchi, V. D.; Xie, H. X.; de Boer, B.; Koster, L. J. A.; Blom, P. W. M. *Adv. Funct. Mater.* **2006**, *16*, 699−708.
(15) van Eijk, C. W. E. *Phys. Med. Biol.* **2002**, *47*, R85−R106.
(16) Gelinck, G. H.; Kumar, A.; Moet, D.; van der Steen, J. L.; Shafique, U.; Malinowski, P. E.; Myny, K.; Rand, B. P.; Simon, M.; Rutten, W.; Douglas, A.; Jorritsma, J.; Heremans, P.; Andriessen, R. *Org. Electron.* **2013**, *14*, 2602−2609.
(17) Shrotriya, V.; Li, G.; Yao, Y.; Chu, C. W.; Yang, Y. *Appl. Phys. Lett.* **2006**, *88*, 073508.
(18) Wang, F. X.; Qiao, X. F.; Xiong, T.; Ma, D. G. *Org. Electron.* **2008**, *9*, 985−993.
(19) Li, G.; Shrotriya, V.; Huang, J. S.; Yao, Y.; Moriarty, T.; Emery, K.; Yang, Y. *Nat. Mater.* **2005**, *4*, 864−868.
(20) Yu, G.; Gao, J.; Hummelen, J. C.; Wudl, F.; Heeger, A. J. *Science* **1995**, *270*, 1789−1791.
(21) Arca, F.; Tedde, S. F.; Sramek, M.; Rauh, J.; Lugli, P.; Hayden, O. *Sci. Rep* **2013**, *3*, 1324.
(22) He, Z. C.; Zhong, C. M.; Huang, X.; Wong, W. Y.; Wu, H. B.; Chen, L. W.; Su, S. J.; Cao, Y. *Adv. Mater.* **2011**, *23*, 4636−4643.
(23) Sun, Y. M.; Takacs, C. J.; Cowan, S. R.; Seo, J. H.; Gong, X.; Roy, A.; Heeger, A. J. *Adv. Mater.* **2011**, *23*, 2226−2230.
(24) Tedde, S. F.; Kern, J.; Sterzl, T.; Furst, J.; Lugli, P.; Hayden, O. *Nano Lett.* **2009**, *9*, 980−983.
(25) Takei, K.; Takahashi, T.; Ho, J. C.; Ko, H.; Gillies, A. G.; Leu, P. W.; Fearing, R. S.; Javey, A. *Nat. Mater.* **2010**, *9*, 821−826.
(26) Tee, B.; Wang, C.; Allen, R.; Bao, Z. *Nat. Nanotechnol.* **2012**, *7*, 825−832.
(27) Someya, T.; Kato, Y.; Sekitani, T.; Iba, S.; Noguchi, Y.; Murase, Y.; Kawaguchi, H.; Sakurai, T. *Proc. Natl. Acad. Sci. U.S.A.* **2005**, *102*, 12289−12290.
(28) Kim, D. H.; Lu, N.; Ma, R.; Kim, Y. S.; Kim, R. H.; Wang, S.; Wu, J.; Won, S. M.; Tao, H.; Islam, A.; Yu, K. J.; Kim, T. I.; Chowdhury, R.; Ying, M.; Xu, L.; Li, M.; Chung, H. J.; Keum, H.; McCormick, M.; Liu, P.; Zhang, Y. W.; Omenetto, F. G.; Huang, Y.; Coleman, T.; Rogers, J. A. *Science* **2011**, *333*, 838−843.

Carbon Nanotube Active-Matrix Backplanes for Mechanically Flexible, Visible Light and X-ray Imagers

Toshitake Takahashi[1,2,3,*], Zhibin Yu[1,2,3,*], Kevin Chen[1,2,3], Daisuke Kiriya[1,2,3], Chuan Wang[1,2,3⊥], Kuniharu Takei[1,2,3,+], Hiroshi Shiraki[1,2,3], Teresa Chen[4], Biwu Ma[3,4,‡] and Ali Javey[1,2,3†]

[1] Electrical Engineering and Computer Sciences, University of California, Berkeley, CA 94702
[2]Berkeley Sensor and Actuator Center, University of California, Berkeley, CA 94720
[3]Materials Sciences Division, Lawrence Berkeley National Laboratory, Berkeley, CA 94720
[4]The Molecular Foundry, Lawrence Berkeley National Laboratory, Berkeley, CA 94720
[⊥]Present address: Electrical and Computer Engineering, Michigan State University, East Lansing, Michigan 48824
[+]Present address: Physics and Electronics, Osaka Prefecture University, Osaka 588-8531, JAPAN
[‡] Present address: Chemical and Biomedical Engineering, Florida State University, Tallahassee, FL 32310
[*]Authors with equal contribution

† Corresponding Author: ajavey@eecs.berkeley.edu

Supporting Information

Mechanical flexibility of organic photodiodes:

The mechanical flexibility of the nanotube TFT backplane has been demonstrated in our previous work – exhibiting minimal change in electrical performance as a function of bending radius[1]. Here, we characterized the mechanical flexibility of our organic photodiodes. The dark current exhibits no measurable response to bending down to a radius of 2 mm (Fig. S1). A slight change in the photocurrent is observed as a function of bending which may be attributed to the change in surface reflectance and effective light intensity illuminated on OPDs.

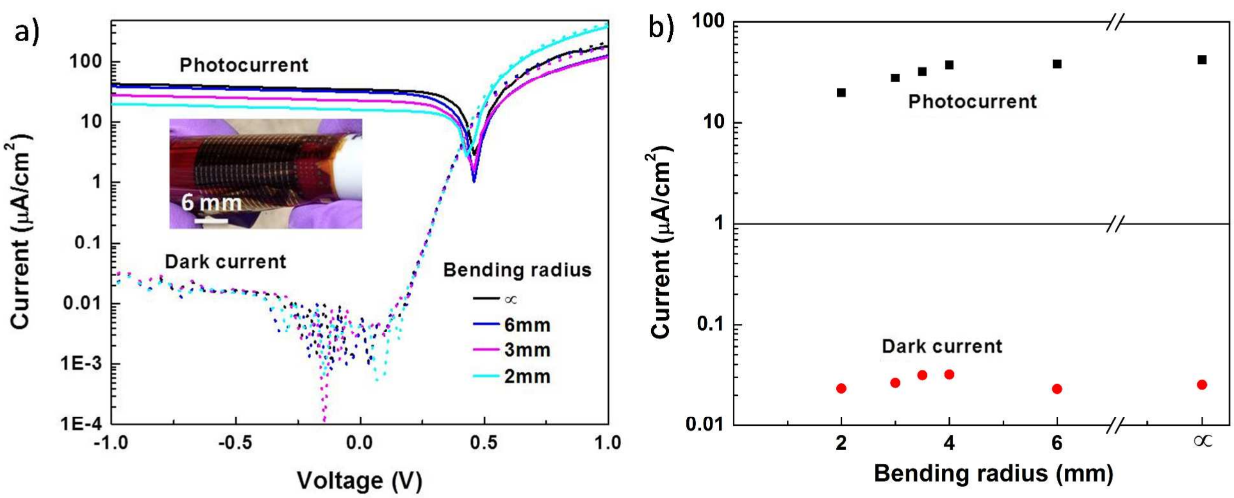

Figure S1. Characterization of an organic photodiode on a PI substrate as a function of bending radius. a) I-V curves under light illumination with an intensity of 500 μW/cm^2 and λ=535 nm (solid lines), and dark condition (dotted lines). b) Photocurrent (top) and dark current (bottom) as a function of bending radius.

References:

1. Wang, C.; Chien, J. C.; Takei, K.; Takahashi, T.; Nah, J.; Niknejad, A. M.; Javey, A. *Nano Lett.* **2012,** *12*, 1527-1533.